

Investigation of a Low-Profile Planar Monolayer UWB Antenna with an Open Slot for Bandwidth Enhancement

Aliakbar Dastranj^{1, *} and Bijan Abbasi-Arand²

Abstract—A low-profile planar monolayer antenna for ultra-wideband (UWB) operation is presented. To achieve a UWB performance along with a compact size, a hybrid square-circular radiator and a rectangular open slotted ground plane with two symmetrical I-shaped tuning stubs are proposed. The antenna is fed by a coplanar waveguide line and has a small size of $44 \times 32 \times 1.6 \text{ mm}^3$. The prototype of the proposed antenna was fabricated and tested in an anechoic chamber. The simulated and measured results show good agreement over the entire ultra-wide bandwidth. The measured results indicate that the proposed antenna can provide a wide impedance bandwidth of more than 154% from 1.7 to 13.3 GHz with -10-dB reflection coefficient. In addition, it is demonstrated that by introducing several antenna designs, the impedance bandwidth can be improved from 43% to 154%. Besides several mechanical advantages, such as compact in size, easy fabrication, and monolayer configuration without any back ground plane, the proposed antenna also shows a good performance in its radiation characteristics and time-domain behaviors. The measured results in both frequency and time domains prove that the proposed antenna can be used in a wide range of UWB applications.

1. INTRODUCTION

Modern wireless ultra-wideband (UWB) communication systems have received considerable attention owing to their high data rates, great capacity, low complexity and low operating power level [1–5]. In these systems, high-performance antennas are required to have the characteristics of both UWB and low-profile. These requirements provide a challenging list of specifications that demand innovation in antenna designs. Therefore, various configurations have been presented to enhance operating bandwidths, among which planar slot antennas have been regarded as popular and suitable candidates due to their advantages of broad bandwidth, simple structure, low cost, easy fabrication and easy integration in active components and monolithic microwave integrated circuits [6–9].

In the last few years, to enhance the impedance bandwidth of printed slot antennas, different methods have been presented. One technique is to use several geometries of slots [10–18], and the other methods use different turning stubs to achieve wideband performance [19, 20]. Among several slot geometries worthwhile mentioning are square [10], triangle [11], rectangle [12], ellipse and circle [13], rhombus [14], fractal [15], annular-ring [16], and binomial-curve [17]. The impedance bandwidths of these antennas are less than 104%. A round-corner rectangular wide-slot antenna with a size of $68 \times 50 \text{ mm}^2$ is proposed in [18]. The impedance bandwidth of the antenna with -10-dB reflection coefficient is almost two octaves from 2.08 to 8.25 GHz. In [19], by using a coplanar waveguide (CPW) feed with a widened tuning stub, a square slot antenna with dimensions of $72 \text{ mm} \times 72 \text{ mm}$ can yield a bandwidth of 60%. The design of a UWB CPW-fed slot antenna etched on a 0.813-mm-thick substrate with a U-shaped tuning stub for bandwidth enhancement is presented in [20]. It features an impedance

Received 7 October 2015, Accepted 3 November 2015, Scheduled 18 November 2015

* Corresponding author: Aliakbar Dastranj (dastranj@yu.ac.ir).

¹ Electrical Engineering Department, Faculty of Engineering, Yasouj University, Yasouj, Iran. ² Communication Engineering Department, Faculty of Electrical and Computer Engineering, Tarbiat Modares University, Tehran, Iran.

bandwidth of 110% and bidirectional radiation patterns with an average gain about 2 dBi. Two printed slot antennas with equal sizes of $110\text{ mm} \times 110\text{ mm}$ and impedance bandwidths of 120% (1.82 to 7.23 GHz) and 110% (2.42 to 8.48 GHz) are presented in [21]. In [22], a printed slot antenna loaded with small heptagonal slots is investigated. The small perturbations are added in the corners of the main slot antenna to provide a multiresonance operation. As a result, a wide impedance bandwidth of 105.3% is achieved. An open-slot antenna with a wide impedance bandwidth of 122% is designed in [23]. Two bevels are cut on an asymmetrical rectangular patch to improve the impedance bandwidth. In [24], based on a rotated square slot resonator, a printed slot antenna with a parasitic patch for bandwidth enhancement is proposed. By properly choosing a suitable slot shape, embedding a similar parasitic patch shape, and tuning their dimensions, a wide operating bandwidth ranging from 2.225 to 5.355 GHz is obtained. Also, a compact CPW-fed antenna with a half-elliptical-edged monopole radiator and two symmetrical open-circuit stubs extended from the ground plane is proposed in [25]. Its impedance bandwidth ranges from 3.7 to 10.1 GHz. Recently, two UWB CPW-fed printed antennas with dimensions of $48 \times 42\text{ mm}^2$ and $50 \times 50\text{ mm}^2$ and impedance bandwidths of 125% and 118.8% are reported in [26] and [27], respectively.

In this paper, a bandwidth-enhancement method using a new radiator with a hybrid square-circular configuration and a rectangular open slotted ground plane with a pair of symmetrical I-shaped tuning stubs is introduced to implement a low-profile planar monolayer UWB antenna. It is demonstrated that etching the open slot on the ground plane along with the I-shaped tuning stubs improve the antenna performance corresponding to the intermediate frequencies. The evolution procedure of the proposed antenna is presented, and several designs are experimentally investigated. The measured results agree well with full-wave simulations. Besides several mechanical advantages, such as simple structure, small size ($44 \times 32 \times 1.6\text{ mm}^3$), easy fabrication, and a monolayer configuration without any back ground plane, the proposed antenna also shows a good performance in its radiation characteristics and time-domain behaviors. Moreover, as will be shown in the following, compared with other designs presented in [26] and [27], the designed antenna has a smaller size and wider bandwidth. This comparison verifies the advantages of the designed antenna. The measured impedance bandwidth of the proposed antenna (defined by -10-dB reflection coefficient) is more than 154% from 1.7 to 13.3 GHz. In addition, it is demonstrated that by utilizing several antenna geometries, the impedance bandwidth can be improved from 43% to 154%. The effects of the key structure parameters on the antenna impedance bandwidth are also investigated and discussed. The measured results in both frequency and time domains confirm that the proposed antenna is a good candidate for UWB communication systems.

2. ANTENNA EVOLUTION PROCEDURE AND DESIGN

The configuration and geometrical parameters of the proposed antenna are shown in Figure 1. The antenna is printed on a 1.6-mm-thick substrate of FR4 whose dielectric constant is $\epsilon_r = 4.4$, and loss tangent is 0.02. The overall dimensions of the substrate are $44 \times 32\text{ mm}^2$. The antenna consists of a hybrid square-circular radiator and a rectangular open slotted ground plane with two symmetrical I-shaped tuning stubs. They are all printed on the same side of the substrate, and the other side of the substrate is empty. In Figure 1, it can be seen that the hybrid square-circular radiator is connected to an E-shaped tuning stub. As will be seen later, the combination of the aforementioned two portions results in UWB impedance bandwidth. A $50\ \Omega$ CPW feed line, having a metal strip of width $g = 1.7\text{ mm}$ and a gap of distance $S = 0.3\text{ mm}$, is used to excite the proposed antenna. As shown in this figure, the E-shaped tuning stub terminates the CPW feed line and is asymmetrical with respect to the y -axis. In addition, to further enhance the antenna operational bandwidth, two symmetrical I-shaped tuning stubs are extended from the ground plane.

The evolution procedure of the proposed antenna is shown in Figure 2 in which the models of original antenna, antenna I, and antenna II are given. At the same time, this figure shows how the proposed antenna is designed from the original antenna. The corresponding simulated reflection coefficients are presented in Figure 3, and the geometrical parameters of the antennas are tabulated in Table 1. The numerical analysis and geometry refinement of the proposed antenna are performed by using Ansoft HFSS, a full-wave electromagnetic simulator package based on the finite element method.

The design procedure starts with the design of the original antenna, which consists of a rectangular

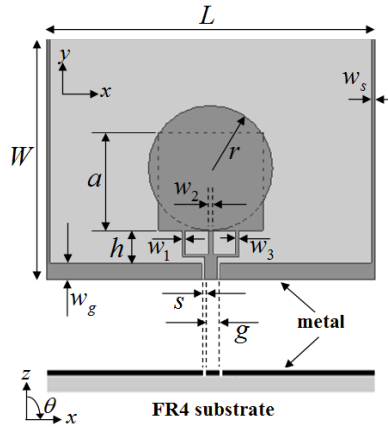


Figure 1. Configuration and geometrical parameters of the proposed antenna.

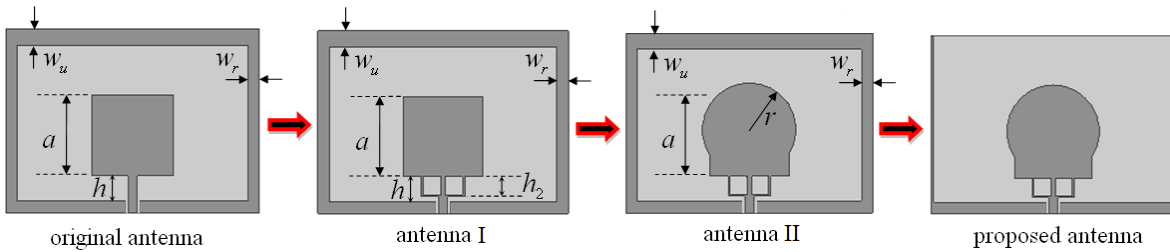


Figure 2. Evolution procedure of the proposed antenna.

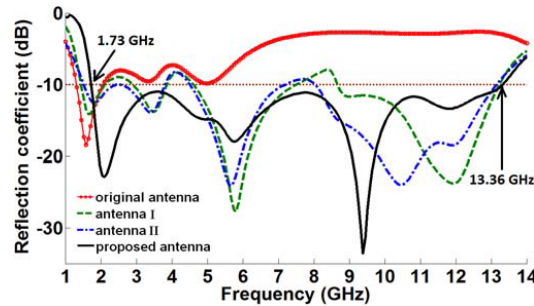


Figure 3. Simulated reflection coefficients of the antennas corresponding to Figure 2.

slotted ground plane and a square radiator with a side length of $a = 13$ mm. The original antenna is excited by a CPW feed line. The spacing between the square radiator and edge of the ground plane is $h = 4.4$ mm. As shown in Figure 3, a -10 -dB reflection coefficient bandwidth about 42% from 1.33 to 2.04 GHz is achieved. After adding an E-shaped tuning stub to the square radiator (antenna I), the antenna can get multiband operation with -10 -dB impedance bandwidths about 36% (1.47–2.12 GHz), 27% (2.92–3.86 GHz), 48% (4.59–7.53 GHz), and 42% (8.63–13.22 GHz), respectively. In the next step, the square radiator is substituted by a hybrid square-circular radiator (antenna II), and as depicted in Figure 3, three impedance bandwidths of 87% (1.50–3.82 GHz), 46% (4.50–7.20 GHz), and 48% (8.04–13.15 GHz) are resulted. In the last step of the antenna design, to further enhance the impedance bandwidth of the antenna, an open slot is etched on the ground plane instead of common rectangular slot, and two I-shaped tuning stubs with equal widths w_s are extended from the ground plane (proposed antenna). As illustrated in Figure 3, the simulated -10 -dB bandwidth of the proposed antenna is more than 154% from 1.73 to 13.36 GHz. Notice that by adding the E-shaped tuning stub to the square radiator, the coupling between the ground plane and the radiator significantly increases.

The left arm of the E-shaped tuning stub controls the generation of resonant modes at about 1.5 and 3.5 GHz, and the middle arm contributes to a resonant mode at about 5.8 GHz, and the resonant mode of the upper band at about 12 GHz is generated, owing to the presence of the right arm. Also, the presence of the hybrid square-circular radiator helps achieve enhanced impedance matching of the two resonant modes in the lower band. As shown in Figure 3, etching the open slot on the ground plane along with the I-shaped tuning stubs (proposed antenna) improves impedance matching of the antenna at the intermediate frequencies about 4–10 GHz. The phenomenon behind the I-shaped stubs is that at microwave frequencies, they act as two capacitor-fed monopoles in the aforementioned frequency band.

The surface current distributions on the radiator and the stubs at 2, 5.8, and 9.4 GHz are illustrated in Figure 4. It can be seen that the lower frequency resonance is dominated by the E-shaped tuning stub. On the other hand, the middle and higher frequency resonances are more determined by the hybrid square-circular radiator and the I-shaped tuning stubs. The surface current distribution discussed above clearly shows that the hybrid radiator, E-shaped stub, and I-shaped stubs collaboratively establish the UWB performance of the antenna.

To further investigate the antenna impedance behavior, the simulated input impedances on Smith charts of the original antenna, antenna I, antenna II, and the proposed antenna are shown in Figure 5. Figure 5(a) depicts impedance locus of original antenna in which the intersect points of impedance locus with $|S_{11}| = -10$ dB circle are highlighted. It is seen that a little portion of impedance locus from

Table 1. Geometrical parameters of the antennas.

Parameter	Original antenna	Antenna I	Antenna II	Proposed antenna
	Value (mm)			
L	44	44	44	44
W	32	32	32	32
w_g	2.1	2.1	2.1	2.1
a	13	13	13	13
h	4.4	4.4	4.4	4.4
w_r	2	2	2	—
w_u	2.9	2.9	2.9	—
w_1	—	0.3	0.3	0.3
w_2	—	0.7	0.7	0.7
w_3	—	0.35	0.35	0.35
h_2	—	3.5	3.5	3.5
r	—	—	8.32	8.32
w_s	—	—	—	0.5

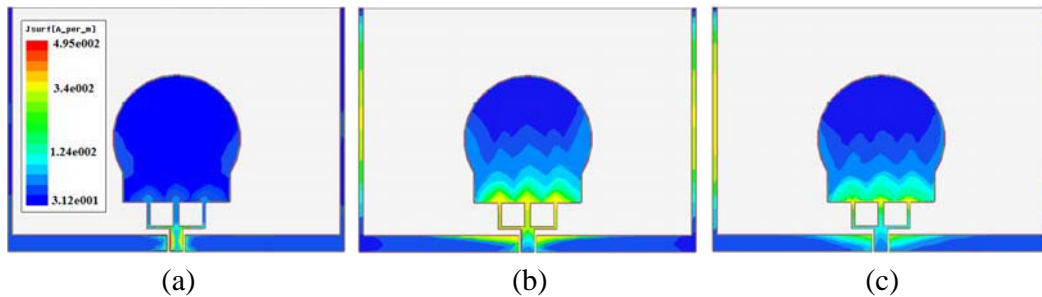


Figure 4. Simulated surface current distributions of the different resonant frequencies, (a) 2, (b) 5.8, and (c) 9.4 GHz.

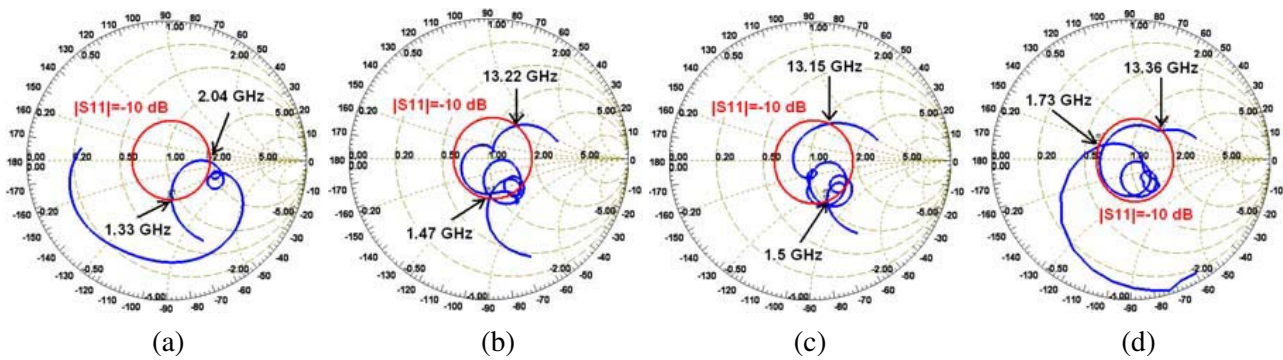


Figure 5. Simulated input impedances on Smith charts of the antennas, (a) original antenna, (b) antenna I, (c) antenna II, (d) proposed antenna.

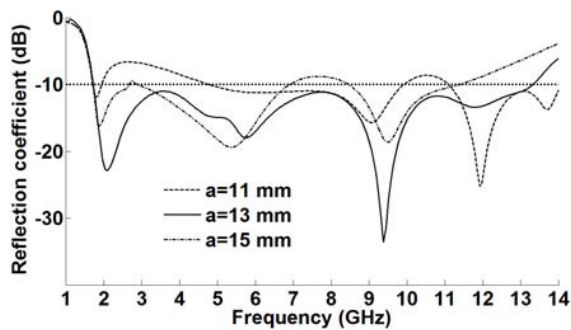


Figure 6. Effects of different side length a on the impedance bandwidth of the proposed antenna. Other geometrical parameters are the same as in Table 1.

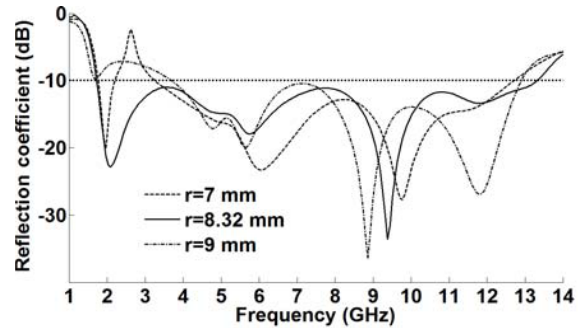


Figure 7. Simulated reflection coefficient curves for different values of radius r . Other geometrical parameters are the same as in Table 1.

1.33 GHz to 2.04 GHz is inside the $|S_{11}| = -10$ dB circle, which is narrow and not sufficient for UWB applications. Figures 5(b) and 5(c) show the impedance loci of antenna I and antenna II, respectively. As illustrated in these figures, four loops on the Smith charts are formed, and major parts of these loops are outside the $|S_{11}| = -10$ dB circle, indicating that these antennas provide multiband operation with -10 -dB reflection coefficient. The simulated input impedance on a Smith chart of the proposed antenna is illustrated in Figure 5(d). This figure shows three loops on the Smith chart, which are related to three resonant frequencies illustrated on the reflection coefficient plot of Figure 3. Moreover, it can be observed that these loops are completely inside the $|S_{11}| = -10$ dB circle, and the proposed antenna has a simulated -10 -dB impedance bandwidth ranging from 1.73 to 13.36 GHz.

3. NUMERICAL SENSITIVITY ANALYSIS

In this section, an extensive numerical sensitivity analysis is conducted to understand the influences of different dimensional parameters on the performance of the proposed antenna. Results show that the side length a and radius r of the hybrid square-circular radiator, width of the I-shaped tuning stubs w_s , and three parameters of the E-shaped tuning stub (i.e., w_1 , w_2 , and w_3) affect the broadband operation of the proposed antenna most effectively.

Figure 6 shows the simulated reflection coefficient curves for different values of side length a while the other parameters of the antenna are kept fixed. As shown in this figure, the reflection coefficient deteriorates within the whole band as a changes. The optimum value of this parameter for maximum impedance bandwidth is 13 mm.

The comparison of the simulated reflection coefficient curves versus frequency for various radii r is presented in Figure 7. It can be observed that the lower and higher end frequencies are largely

dependent on radius r . The best bandwidth performance is achieved when this parameter is chosen to be $r = 8.32$ mm.

The effect of various widths w_s on the impedance bandwidth of the proposed antenna is displayed in Figure 8. It is seen that through varying factor w_s from 0.5 to 2 mm, the antenna reflection coefficient corresponding to the lower and middle frequencies is increased. The best value of w_s for optimum impedance bandwidth is 0.5 mm.

Next, the effects of the E-shaped tuning stub dimensions on the impedance matching of the proposed antenna are studied. Figures 9(a), (b), and (c) depict the influences of different widths w_1 , w_2 , and w_3 of the left, middle, and right branches of the E-shaped tuning stub, respectively, on the impedance bandwidth of the antenna. Referring to these figures, it is observed that these geometrical parameters affect the lower end frequency of the bandwidth significantly, and the upper edge of the bandwidth is deteriorated slightly. The optimal widths of w_1 , w_2 , and w_3 are 0.3, 0.7, and 0.35 mm, respectively.

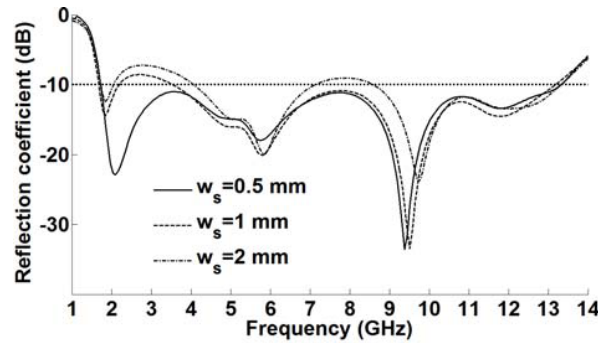


Figure 8. Effects of various widths w_s on the impedance bandwidth of the proposed antenna. Other geometrical parameters are the same as in Table 1.

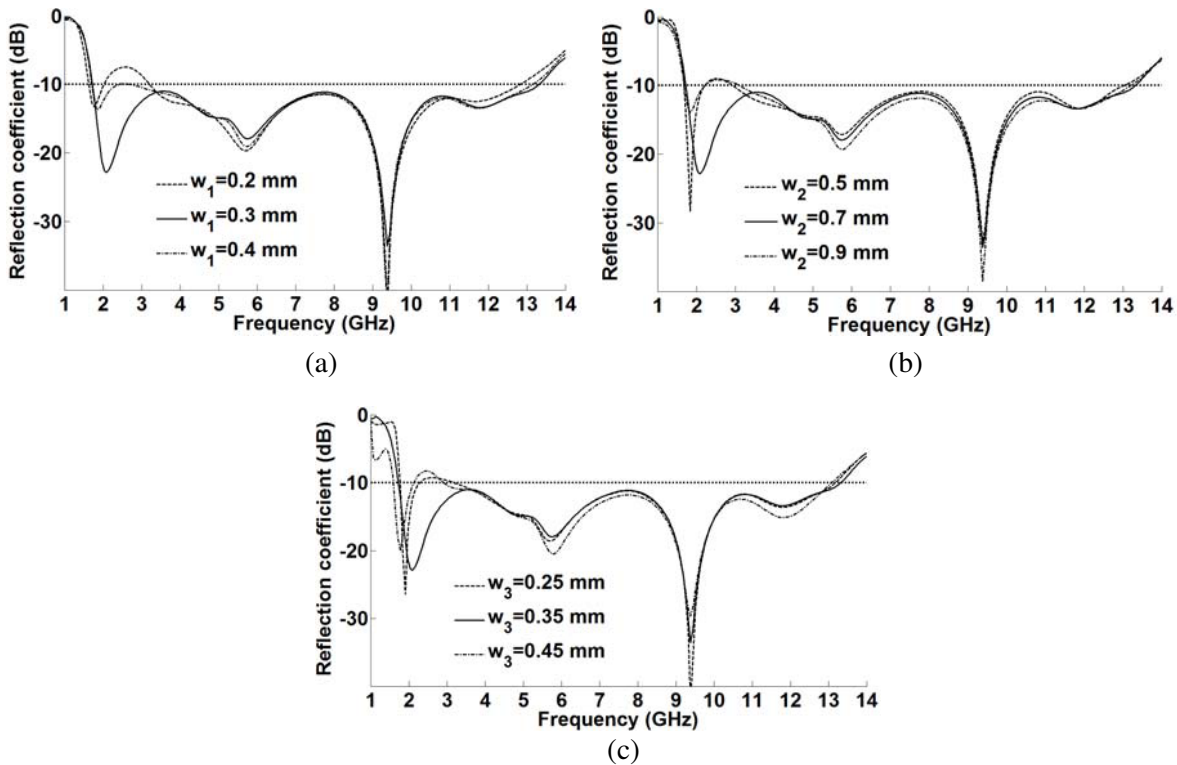


Figure 9. Simulated reflection coefficient curves of the proposed antenna for different values of widths (a) w_1 , (b) w_2 , and (c) w_3 . In each case, other geometrical parameters are the same as in Table 1.

4. EXPERIMENTAL VERIFICATION

To confirm the simulation results, the designed antennas were fabricated and tested inside a microwave anechoic chamber. Figure 10 shows the fabricated prototypes of the antennas. In this section, the measured results in both frequency and time domains are presented and compared with the simulations.

4.1. Frequency-domain Characteristics

The comparison of measured and simulated reflection coefficient curves of the several antennas is presented in Figure 11. The measured results show good agreement with the simulated ones that validate the design procedure. As illustrated in Figure 11(a), the measured impedance bandwidth of the original antenna with -10 -dB reflection coefficient is from 1.34 to 2.08 GHz (43%). Referring to Figure 11(b), it can be observed that antenna I provides quadruple-band operation with -10 -dB impedance bandwidths of about 33% (1.51–2.12 GHz), 33% (2.75–3.83 GHz), 45% (4.59–7.31 GHz), and 45% (8.25–13.12 GHz). From Figure 11(c), it is seen that antenna II has three relative impedance bandwidths with -10 -dB reflection coefficient about 86% (1.51–3.80 GHz), 46% (4.50–7.20 GHz), and 45% (8.04–13.14 GHz). From Figure 11(d), it is seen that the proposed antenna has two relative impedance bandwidths with -10 -dB reflection coefficient about 86% (1.51–3.80 GHz), 46% (4.50–7.20 GHz), and 45% (8.04–13.14 GHz).



Figure 10. Photograph of the fabricated antennas.

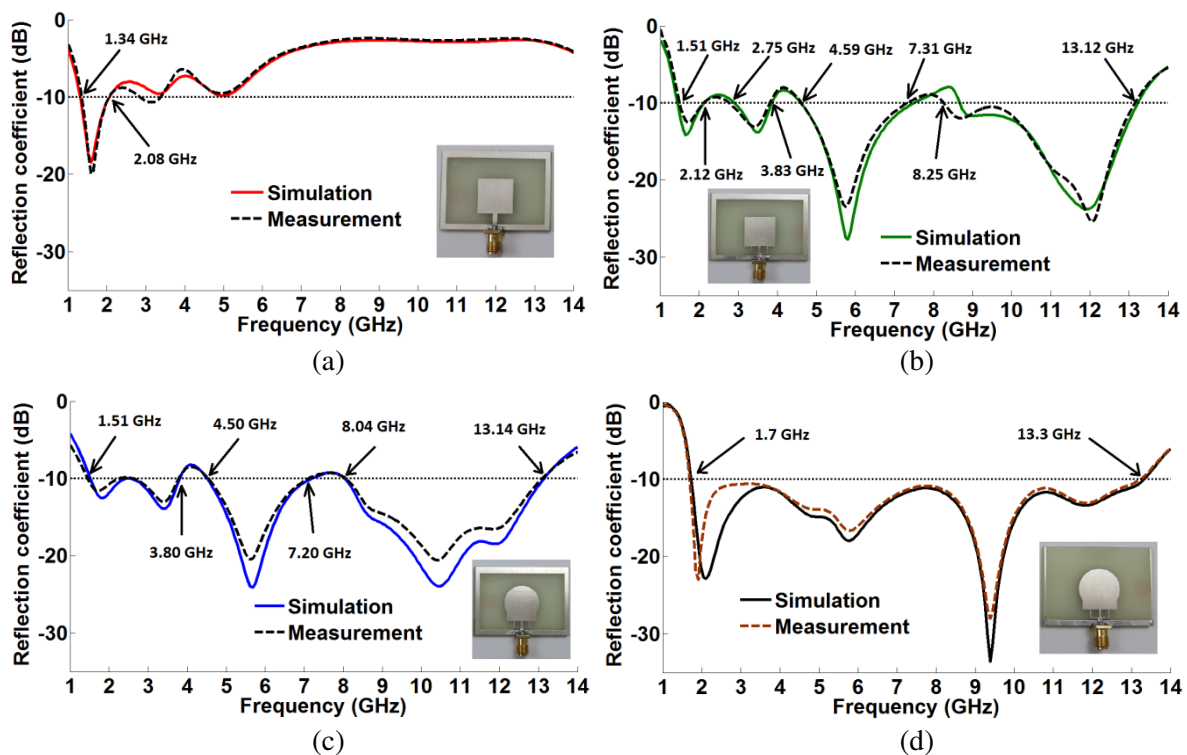


Figure 11. Simulated and measured reflection coefficient curves of the antennas, (a) original antenna, (b) antenna I, (c) antenna II, (d) proposed antenna.

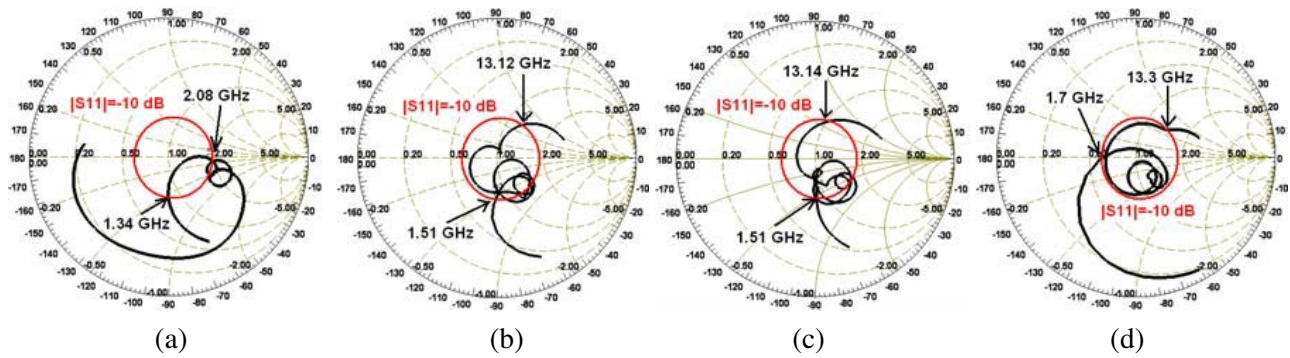


Figure 12. Measured impedance loci of the antennas, (a) original antenna, (b) antenna I, (c) antenna II, (d) proposed antenna.

48% (8.04–13.14 GHz), respectively. As presented in Figure 11(d), the measured -10 -dB bandwidth of the proposed antenna is more than 154% from 1.7 to 13.3 GHz, which agrees well with the simulation result from 1.73 to 13.36 GHz. This bandwidth enhancement is obtained by etching the open slot on the ground plane with two I-shaped tuning stubs.

The measured impedance loci of the original antenna, antenna I, antenna II, and the proposed antenna are shown in Figure 12. As presented in Figure 12(a), the impedance locus of the original antenna for the frequency range of 1.34–2.08 GHz is located on the inner side of $|S_{11}| = -10$ dB circle. Also, Figures 12(b) and 12(c) indicate the multiband operation (with -10 -dB reflection coefficient) of antenna I and antenna II, respectively. The measured input impedance on a Smith chart of the proposed antenna is presented in Figure 12(d). As expected, for the frequencies between 1.7 and 13.3 GHz, there are three resonant impedance loops on the Smith chart which are completely inside the $|S_{11}| = -10$ dB circle. It is seen that the impedance locus of Figure 12(d) is compatible with the reflection coefficient plotted in Figure 11(d).

Comparison of the simulated and measured co- and cross-polar far-field E -plane (y - z plane) and H -plane (x - z plane) radiation patterns of the proposed antenna at 4, 7, and 10 GHz are presented in Figure 13. It is seen that the experimental results show good agreement with the simulation data. From these results, it can be observed that all patterns exhibit bidirectional properties and that E -plane patterns are slightly tilted at higher frequencies due to the undesired higher order modes. These patterns show that the proposed antenna provides linear polarization with cross-polarization level about 30 dB lower than the co-polarization level at boresight in all of the measured radiation patterns. The cross-polarization levels at other directions are also small, indicating excellent polarization purity. Figure 14 shows the measured and simulated maximum realized gains of the proposed antenna at boresight direction within 2–13 GHz frequency range. The measured gain variation is observed to be less than 2.4 dBi, with a maximum gain of about 5.0 dBi which occurs at 7 GHz. The difference between simulation and measurement at 10 GHz is due to the measurement errors and test equipment's.

4.2. Time-Domain Characteristics

In the last step of verification, the distortionless time domain performance of the proposed antenna was confirmed by the measured and simulated group delay shown in Figure 15. For this purpose, the transmitting and receiving antennas were separated by a distance of 40 cm, and the group delay for both side-by-side and face-to-face configurations was investigated. As illustrated in this figure, the group delay is almost constant over the whole bandwidth, except at 1.9 and 9.4 GHz, and both plots show discontinuities, possibly due to the resonances at these frequencies. However, the variation (peak to peak deviation) of the group delay for both configurations is less than 1.5 ns in the entire operating bandwidth. Reasonable agreement has been achieved between simulated and measured results. The results indicate that the proposed antenna is reliable so that a transmitted signal will not be seriously distorted by it. Thus, the designed antenna is suitable for UWB communication applications.

It is worth mentioning that the proposed antenna has an overall size of $44 \times 32 \text{ mm}^2$, which is

less than the size of the presented antennas in [26] and [27] with dimensions of $48 \times 42 \text{ mm}^2$ and $50 \times 50 \text{ mm}^2$, respectively. The impedance bandwidths of the antennas in [26] and [27] are 125% (3–10 GHz) and 118.8% (2.8–11 GHz), respectively, whereas the impedance bandwidth of the antenna in this design is more than 154% (1.7–13.3 GHz). This comparison verifies the advantages of the proposed design procedure.

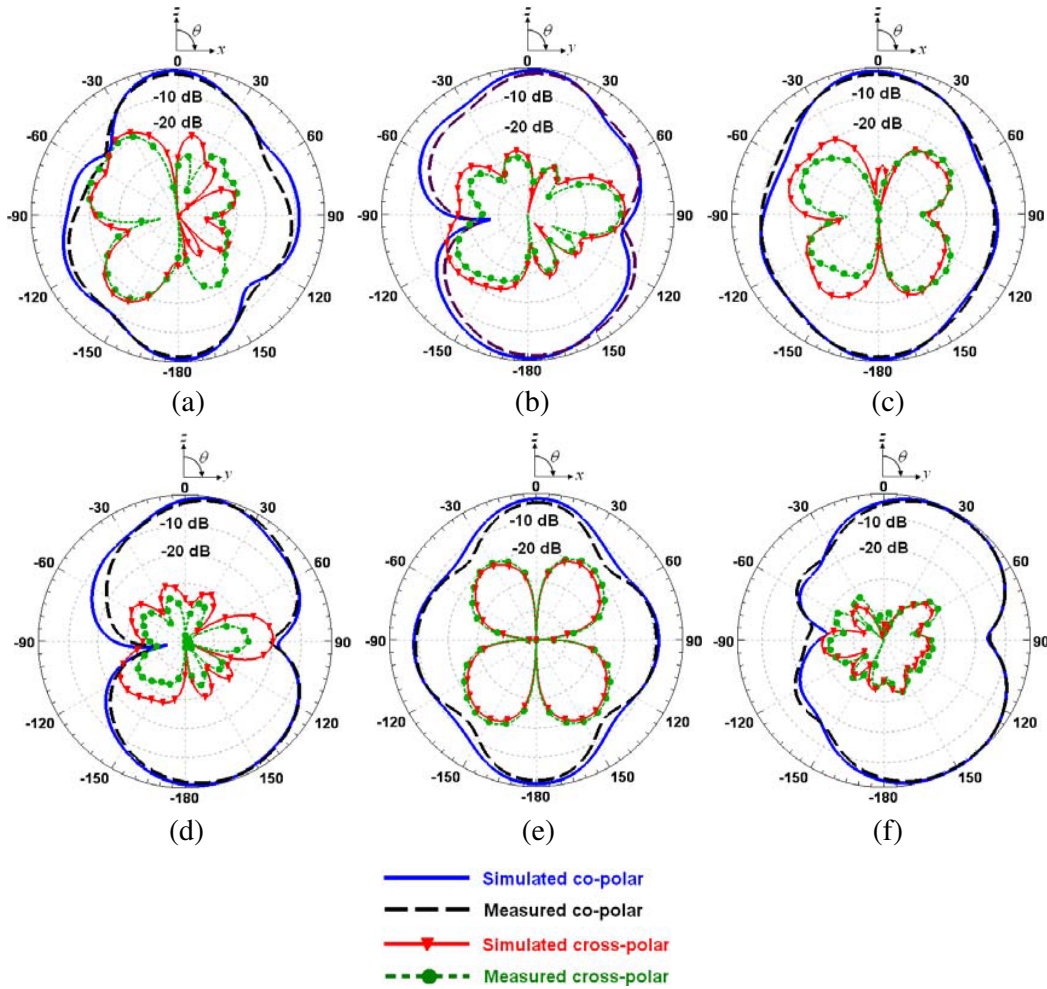


Figure 13. Simulated and measured far-field patterns of the proposed antenna, (a) *H*-plane at 4 GHz, (b) *E*-plane at 4 GHz, (c) *H*-plane at 7 GHz, (d) *E*-plane at 7 GHz, (e) *H*-plane at 10 GHz, (f) *E*-plane at 10 GHz.

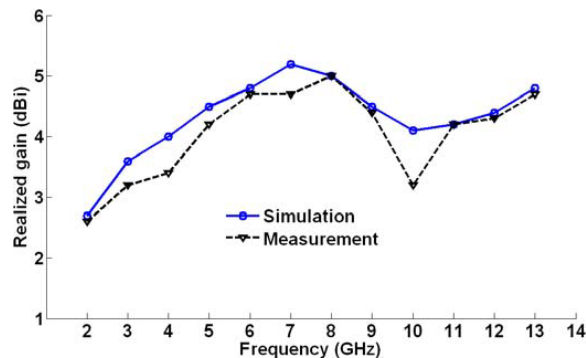


Figure 14. Simulated and measured maximum realized gains of the proposed antenna.

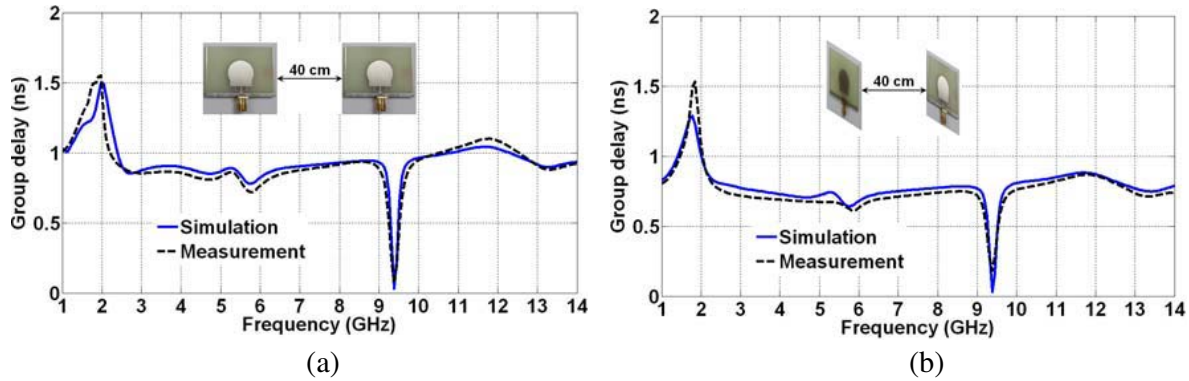


Figure 15. Simulated and measured group delay of the proposed antenna, (a) side-by-side configuration, (b) face-to-face configuration.

5. CONCLUSION

In this paper, a low-profile planar monolayer CPW-fed UWB antenna is presented. In order to jointly achieve a UWB performance with a compact size, a hybrid square-circular radiator and rectangular open slotted ground plane with two symmetrical I-shaped tuning stubs are utilized. The evolution procedure of the proposed antenna is presented and several designs are experimentally investigated. The measured results are in good agreement with the full-wave simulations. The measured impedance bandwidth of the proposed antenna (defined by -10 -dB reflection coefficient) is more than 154% from 1.7 to 13.3 GHz. Moreover, it is shown that the impedance bandwidth can be enhanced from 43% to 154% by using different antenna types. Also, a numerical sensitivity analysis has been carried out to understand the effects of the key geometrical parameters on the antenna impedance bandwidth. Besides several mechanical features, such as simple structure, compact size ($44 \times 32 \times 1.6 \text{ mm}^3$), easy fabrication, and monolayer configuration without any back ground plane, the proposed antenna also shows a good performance in its radiation characteristics and time domain behaviors. It is demonstrated that compared with the designs in [26] and [27], the proposed antenna has a smaller size and wider impedance bandwidth. The measured results in both frequency and time domains confirm that the proposed antenna is a good candidate for UWB communication systems.

REFERENCES

1. Fan, S. T., Y. Z. Yin, B. Lee, W. Hu, and X. Yang, "Bandwidth enhancement of a printed slot antenna with two parasitic patches," *IEEE Antennas and Wireless Propagation Letters*, Vol. 11, 1230–1233, 2012.
2. Li, G., H. Zhai, T. Li, X. Y. Ma, and C.-H. Liang, "Design of a compact UWB antenna integrated with GSM/WCDMA/WLAN bands," *Progress In Electromagnetics Research*, Vol. 136, 409–419, 2013.
3. Lizzi, L., G. Oliveri, and A. Massa, "A time-domain approach to the synthesis of UWB antenna systems," *Progress In Electromagnetics Research*, Vol. 122, 557–575, 2012.
4. Zhang, Z. and Y. H. Lee, "A robust CAD tool for integrated design of UWB antenna system," *Progress In Electromagnetics Research*, Vol. 112, 441–457, 2011.
5. Habib, M. A., A. Bostani, A. Djaiz, M. Nedil, M. C. E. Yagoub, and T. A. Denidni, "Ultra wideband CPW-fed aperture antenna with WLAN band rejection," *Progress In Electromagnetics Research*, Vol. 106, 17–31, 2010.
6. Yu, C.-C. and X.-C. Lin, "A wideband single chip inductor-loaded CPW-fed inductive slot antenna," *IEEE Transactions on Antennas and Propagation*, Vol. 56, No. 5, 1498–1501, May 2008.
7. Li, X. L., Y.-Z. Yin, P. A. Liu, J. H. Wang, and B. Xu, "A CPW-fed dual band-notched UWB

- antenna with a pair of bended dual-L-shape parasitic branches,” *Progress In Electromagnetics Research*, Vol. 136, 623–634, 2013.
8. Chen, D. and C.-H. Cheng, “A novel compact ultra-wideband (UWB) wide slot antenna with via holes,” *Progress In Electromagnetics Research*, Vol. 94, 343–349, 2009.
 9. Jiao, J.-J., G. Zhao, F.-S. Zhang, H.-W. Yuan, and Y.-C. Jiao, “A broadband CPW-fed T-shape slot antenna,” *Progress In Electromagnetics Research*, Vol. 76, 237–242, 2007.
 10. Chiou, J.-Y., J.-Y. Sze, and K.-L. Wong, “A broad-band CPW-fed striploaded square slot antenna,” *IEEE Transactions on Antennas and Propagation*, Vol. 51, No. 4, 719–721, Apr. 2003.
 11. Chen, W. S. and F. M. Hsieh, “A broadband design for a printed isosceles triangular slot antenna for wireless communications,” *Microwave Journal*, Vol. 48, No. 7, 98–112, Jul. 2005.
 12. Chen, W. S., “A novel broadband design of a printed rectangular slot antenna for wireless communications,” *Microwave Journal*, Vol. 49, No. 1, 122–130, Jul. 2006.
 13. Li, P., J. Liang, and X. Chen, “Study of printed elliptical/circular slot antennas for ultrawideband applications,” *IEEE Transactions on Antennas and Propagation*, Vol. 54, No. 6, 1670–1675, Jun. 2006.
 14. Jan, J. Y. and L. C. Wang, “A study on broadband printed slot antennas with regular rhombus slots,” *Proc. IEEE Region 10 Conference (TENCON)*, 1–3, Taipei, Taiwan, Oct. 30–Nov. 2, 2007.
 15. Krishna, D. D., M. Gopikrishna, C. K. Anandan, P. Mohanan, and K. Vasudevan, “CPW-fed koch fractal slot antenna for WLAN/WiMAX applications,” *IEEE Antennas and Wireless Propagation Letters*, Vol. 7, 389–392, 2008.
 16. Sze, J.-Y., C.-I. G. Hsu, and S.-C. Hsu, “Design of a compact dual-band annular-ring slot antenna,” *IEEE Antennas and Wireless Propagation Letters*, Vol. 6, 423–426, 2007.
 17. Liang, X. L., T. A. Denidni, L. N. Zhang, R. H. Jin, J. P. Geng, and Q. Yu, “Printed binomial-curved slot antennas for various wideband applications,” *IEEE Transactions on Microwave Theory and Techniques*, Vol. 59, No. 4, 1058–1065, Apr. 2011.
 18. Lee, H. L., H. J. Lee, J. G. Yook, and H. K. Park, “Broadband planar antenna having round corner rectangular wide slot,” *Proc. IEEE Antennas and Propagation Society Int. Symp.*, Vol. 2, 460–463, Jun. 16–21, 2002.
 19. Chen, H.-D., “Broadband CPW-fed square slot antennas with a widened tuning stub,” *IEEE Transactions on Antennas and Propagation*, Vol. 51, No. 4, 1982–1986, Aug. 2003.
 20. Chair, R., A. A. Kishk, and K. F. Lee, “Ultrawideband coplanar waveguide-fed rectangular slot antenna,” *IEEE Antennas and Wireless Propagation Letters*, Vol. 3, 227–229, 2004.
 21. Liu, Y. F., K. L. Lau, Q. Xue, and C. H. Chan, “Experimental studies of printed wide-slot antenna for wide-band applications,” *IEEE Antennas and Wireless Propagation Letters*, Vol. 3, 273–275, 2004.
 22. Eskandari, H., M. R. Booket, M. Kamyab, and M. Veysi, “Investigation on a class of wideband printed slot antenna,” *IEEE Antennas and Wireless Propagation Letters*, Vol. 9, 1221–1224, 2010.
 23. Liu, W. X., Y. Z. Yin, W. L. Xu, and S. L. Zuo, “Compact open-slot antenna with bandwidth enhancement,” *IEEE Antennas and Wireless Propagation Letters*, Vol. 10, 850–1224, 2011.
 24. Sung, Y., “Bandwidth enhancement of a microstrip line-fed printed wide-slot antenna with a parasitic center patch,” *IEEE Transactions on Antennas and Propagation*, Vol. 60, No. 4, 1712–1716, Apr. 2012.
 25. Xu, K., Z. Zhu, H. Li, J. Huangfu, C. Li, and L. Ran, “A printed single-layer UWB monopole antenna with extended ground plane stubs,” *IEEE Antennas and Wireless Propagation Letters*, Vol. 12, 237–240, 2013.
 26. Unnikrishnan, D., D. Kaddour, S. Tedjini, E. Bihar, and M. Saadaoui, “CPW-fed inkjet printed UWB antenna on ABS-PC for integration in molded interconnect devices technology,” *IEEE Antennas and Wireless Propagation Letters*, Vol. 14, 1124–1128, 2015.
 27. Siddiqui, J. Y., C. Saha, and Y. M. M. Antar, “A novel ultrawideband (UWB) printed antenna with a dual complementary characteristic,” *IEEE Antennas and Wireless Propagation Letters*, Vol. 14, 974–977, 2015.